Magnetic Anisotropy of Two Cyclic Hexanuclear Fe(III) Clusters Entrapping Alkaline Ions

O. Waldmann,*,† J. Schülein,† R. Koch,† P. Müller,† I. Bernt,‡ R. W. Saalfrank,‡ H. P. Andres,§ H. U. Güdel,§ and P. Allenspach||

Physikalisches Institut III, Universität Erlangen-Nürnberg, D-91058 Erlangen, Germany, Institut für Organische Chemie, Universität Erlangen-Nürnberg, D-91058 Erlangen, Germany, Departement für Chemie und Biochemie, Universität Bern, CH-3000 Bern 9, Switzerland, and Laboratorium für Neutronenstreuung, ETHZ & PSI Villigen, CH-5232 Villigen PSI, Switzerland

Received June 4, 1999

The magnetic anisotropy of the two cyclic hexanuclear Fe(III) clusters $[Li\subset Fe_6L_6]Cl\cdot 6CHCl_3$ and $[Na\subset Fe_6L_6]Cl\cdot 6CHCl_3$, $L = N(CH_2CH_2O)_3$, was investigated. Based on a spin Hamiltonian formalism, the magnetic anisotropy was calculated exactly to first order, i.e., in the strong exchange limit, using Bloch's perturbational approach and irreducible tensor operator techniques. Experimentally, the magnetic anisotropy was investigated by magnetic susceptibility and high-field torque magnetometry of single crystals as well as inelastic neutron scattering. It is demonstrated that torque magnetometry provides a valuable tool for the study of magnetic anisotropy in spin cluster complexes. The experimental data could be accurately reproduced by the calculations, and the different methods yield consistent values for the coupling constants and zero-field-splitting parameters. Both the anisotropy and the exchange interaction parameter are found to increase with increasing Fe−O−Fe angle.

1. Introduction

Dinuclear complexes of magnetic transition and rare earth metal ions have been used extensively for a detailed study of the nature of exchange interactions.[1,2] They serve as molecular model systems for magnets with extended interactions. Magnetostructural correlations have been established in related series of complexes,[3,4] and in some cases the orbital exchange pathways have been identified.[5] In contrast to systems with extended interactions, the effective Hamiltonians describing the magnetic coupling of dinuclear complexes can be solved exactly.

In recent years a new class of high-nuclearity spin clusters (HNSC) has become the focus of very intensive research activity, both by chemists and physicists. At first, this was driven by synthetic chemists coming up with species exhibiting an enormous variety of structures.[6−8] Transition metal and rare earth metal ions as well as organic radicals were used as building blocks for polynuclear species. More recently, it was found that some of these spin clusters exhibit very unusual physical properties. $Mn_{12}O_{12}(O_2CCH_3)_{16}(H_2O)_4$ and $[Fe_8O_2(OH)_{12}(tacn)_6]^{8+}$ with cluster ground states $S = 10$ and $S = 8$, respectively, have become prototypes of this specific class of spin clusters.[9,10] At very low temperatures they exhibit quantum tunneling as well as magnetic hysteresis effects.[11,12]

The synthetic and magnetic properties of several ferric wheels with the number of Fe(III) ions ranging from 6 to 18 have been reported.[7,13−20] They represent ideal model systems for quantum spin chains which are relevant for the calculation of thermodynamic properties of one-dimensional magnetic materials. Recently we reported the new hexanuclear wheels $[Li\subset Fe_6L_6]Cl\cdot 6CHCl_3$ (**1**) and $[Na\subset Fe_6L_6]Cl\cdot 6CHCl_3$ (**2**), $L = N(CH_2CH_2O)_3$.[18] The alkali ion is situated at the center of the hexagonal wheel and stabilizes the complex. The perchlorate salts of the same complexes, $[Li\subset Fe_6L_6]ClO_4\cdot 2MeOH$ (**3**) and $[Na\subset Fe_6L_6]ClO_4\cdot 2MeOH$ (**4**), as well as the alkali free $[Fe_6L_6]\cdot 6MeOH$ (**5**) cluster were synthesized using a different strategy. Their magnetic properties were reported in ref 20.

In the present paper we report a detailed study of the magnetic properties of the Fe_6 clusters **1** and **2**. Besides magnetic susceptibility measurements we applied torque magnetometry

† Physikalisches Institut III, Universität Erlangen-Nürnberg.
‡ Institut für Organische Chemie, Universität Erlangen-Nürnberg.
§ Universität Bern.
|| ETHZ & PSI Villigen.

(1) Kahn, O. W. *Molecular Magnetism*; VCH Publishers: New York, 1993.
(2) Willet, R. D.; Gatteschi, D.; Kahn, O. *Magneto-Structural Correlations in Exchange Coupled Systems*; NATO ASI Series; D. Reidel Publishing Company: Dordrecht, Holland, 1985.
(3) Hatfield, W. E. In ref 2, p 555.
(4) Weihe, H.; Güdel, H.-U. *J. Am. Chem. Soc.* **1997**, *119*, 6539.
(5) McCarthy, P. J.; Güdel, H.-U. *Coord. Chem. Rev.* **1988**, 88, 69.
(6) Benelli, D.; Caneschi, A.; Gatteschi, R. *J. Am. Chem. Soc.* **1993**, *32*, 4797.
(7) Taft, K. L.; Delfs, C. D.; Papaefthymiou, G. C.; Foner, S.; Gatteschi, D.; Lippard, S. J. *J. Am. Chem. Soc.* **1994**, *116*, 823.
(8) Gatteschi, D.; Tsukerblat, B.; Barra, A. L.; Brunel, L. C.; Müller, A.; Döring, J. *Inorg. Chem*. **1993**, *32*, 2114.
(9) Lis, X. *Acta Crystallogr. B* **1980**, *36*, 2042.
(10) Wieghardt, W.; Phol, K.; Jibril, I.; Huttner, G. *Angew. Chem.* **1984**, *23*, 77.
(11) Gatteschi, D.; Caneschi, A.; Pardi, L.; Sessoli, R. *Science* **1994**, *265*, 1054.
(12) Sangregorio, C.; Ohm, T.; Paulsen, C.; Sessoli, R. *Phys. Rev. Lett.* **1997**, *78*, 4645.
(13) Taft, K. L.; Lippard, S. J. *J. Am. Chem. Soc.* **1990**, *112*, 9629.
(14) Caneschi, A.; Cornia, A.; Lippard, S. J. *Angew. Chem.* **1995**, *107*, 511.
(15) Caneschi, A.; Cornia, A.; Fabretti, A. C.; Foner, S.; Gatteschi, D.; Grandi, R.; Schenetti, L. *Chem.−Eur. J.* **1996**, *2*, 1379.
(16) Benelli, C.; Parsons, S.; Solan, G. A.; Winpenny, R. E. P. *Angew. Chem.* **1996**, *108*, 1967
(17) Watton, S. P.; Fuhrmann, P.; Pence, L. E.; Caneshi, A.; Cornia, A.; Abbati, G. L.; Lippard, S. J. *Angew. Chem.* **1997**, *109*, 2917.
(18) Saalfrank, R. W.; Bernt, I.; Uller, E.; Hampel, F. *Angew. Chem.* **1997**, *109*, 2596.
(19) Bernt, I.; Saalfrank, R. W. *Templatgesteuerter Selbstaufbau von Metallacoronaten*; Erlangen, 1997.
(20) Pilawa, B.; Desquiotz, R.; Kelemen, M. T.; Weickenmeier, M.; Geisselman, A. *J. Magn. Magn. Mater.* **1997**, *177−181*, 748.

10.1021/ic9906510 CCC: $18.00
Published on Web 11/20/1999

and inelastic neutron scattering (INS). Torque magnetometry is shown to be of particular value for the study of anisotropy effects in HNSC. The main advantage of the INS technique is that the exchange splitting pattern can be directly determined without applying a magnetic field. From a comparison of our results with those reported for related complexes we recognize a systematic variation of the magnetic parameters as a function of the Fe−O−Fe angle.

2. Sample Preparation and Experimental Techniques

2.1. Synthesis and Characterization of the Samples. 2.1.1. Samples for Magnetization and Torque Measurements. Single crystals of $[Li\subset Fe_6\{N(CH_2CH_2O)_3\}_6]Cl\cdot 6CHCl_3$ (**1**) and $[Na\subset Fe_6\{N(CH_2CH_2O)_3\}_6]Cl\cdot 6CHCl_3$ (**2**) were prepared as previously described.[18] Both **1** and **2** crystallize in the space group $R\bar{3}$, and the cations $[Li\subset Fe_6L_6]^+$ and $[Na\subset Fe_6L_6]^+$ exhibit S_6 molecular symmetry with the six iron atoms forming a regular hexagon. Powder samples were obtained by drying the crystals in a vacuum and thus removing the $CHCl_3$ molecules. Powder samples of **1** and **2** were characterized by X-ray powder diffraction. The hexagonal unit cells are preserved upon drying, but a drastic reduction of the unit cell parameters is observed. *a* and *b* are reduced by about 30%, whereas the reduction along *c* is negligible.

2.1.2. Sample for INS Measurements. Crystals of $[Na\subset Fe_6\{N(CH_2CH_2O)_3\}_6]Cl\cdot 2CH_2Cl_2$ were prepared according to ref 19. It crystallizes in the space group *P*1. The cation $[Na\subset Fe_6L_6]^+$ has C_i symmetry with Fe−Fe distances ranging from 3.21 to 3.23 Å.[19] Vacuum drying of the crystals yielded approximately 6 g of polycrystalline material (**6**). The product was characterized by chemical analysis, magnetic susceptibility and X-ray powder diffraction using the program LAZY PULVERIX[22] and the structural data given in ref 19. The sample turned out to contain two phases in a ratio of about 2:1. The major phase is the correct $[Na\subset Fe_6\{N(CH_2CH_2O)_3\}_6]Cl$ with a triclinic structure similar to the single crystals with CH_2Cl_2. The impurity phase is likely an Fe_5 cluster. This sample would be of minor value for study by magnetic measurements, but it turned out that the impurity features could be clearly identified in the INS spectra, and the data could be interpreted.

2.2. Magnetic Susceptibility. The magnetic moment of powder and crystal samples was measured with a Quantum Design SQUID magnetometer. The temperature range was 1.8−250 K and the maximum field 5.5 T. The susceptibility was determined from the measurements at fields of 0.5 T. The samples were fixed with Apiezon grease in a plastic straw. The background signal of the straw was found to be below the sensitivity of the magnetometer. For the powder samples, the signal of the grease was measured independently. The data were then corrected with an accuracy of 2.5% at 250 K. The weight of the powder samples was typically 5 mg. Using the molecular weights obtained by X-ray crystallography the experimentally determined *g*-factors were significantly lower than the expected value of $g = 2$. This is attributed to the unknown content of solvent molecules. The data were therefore normalized to $g = 2$ by multiplying with $(2/g)^2$. This normalization does not affect the determined coupling constants. For the crystal measurements, a single crystal was selected by light microscopy and then fixed with a very small amount of grease in the plastic straw. The magnetic contribution of the grease could be neglected. Each crystal was measured repeatedly at several mutually perpendicular field directions. The molecular S_6 axis was aligned with an accuracy of ±7° parallel and perpendicular to the magnetic field. The weight of the crystal samples was typically 50 μg. Data were also normalized to $g = 2$ for each measurement. A possible *g*-factor anisotropy is thus overlooked. However, experimentally it was found to be very small in agreement with the theoretical expectation.[23] The determination of an anisotropy contribution due to a zero-field splitting is not affected by this procedure. For each compound at least three powder and three crystal samples were investigated. The data were corrected for the TIP of the Fe(III) ions and the diamagnetic contribution of the ligands which was estimated from Pascal's constants.

2.3. Torque Magnetometry. The torque of crystal samples was measured with a torsion wire magnetometer[23,24] which provides a resolution of 10^{-12} N m $= 10^{-5}$ emu G. The samples were aligned in situ with an accuracy of ±1°. The temperature dependence was measured with an angle of 45° between the molecular S_6 axis and the magnetic field, the field dependence with an angle of 54.7°. The torquemeter was equipped with a calibration coil. The accuracy is ±7%. The torsion wire magnetometer was inserted into a 15 T/17 T cryomagnet system with a variable-temperature insert. Data were corrected for the background of the torsion wire magnetometer, which was measured independently. The contribution of the grease could be neglected. For each compound at least three single crystals were investigated. The weight of the crystal samples was typically 50 μg. The magnitude of the torque in units of N μ_B T was determined with an accuracy of ±10% by measuring the magnetic moment of each crystal with the SQUID magnetometer.

2.4. Inelastic Neutron Scattering. The polycrystalline sample was sealed under helium in an aluminum container of 15 mm diameter and 55 mm length suitable for inelastic neutron-scattering experiments. These were carried out on the triple-axis instrument DrüchaL at the SINQ, PSI Villigen. Wavelength selection in the monochromator was achieved with the (002) reflection of pyrolytic graphite. In the analyzer a cold beryllium filter and a pyrolytic graphite filter were used to fix the wavelength to 21.75 K throughout the experiment. The axes of the spectrometer were chosen to scan the neutron-energy loss region at constant *Q* values of 0.3, 0.5, 1.0, and 1.5 $Å^{-1}$. Temperature stability at 1.8, 10, and 30 K was obtained with a Neocera temperature controller. The data treatment was done with the commercial program Igor Pro 3.10 (Wave metrics).

3. Theory

3.1. Calculation of Energy Splittings and Magnetic Susceptibility. The appropriate spin Hamiltonian for the ground-state energy splittings in a regular hexanuclear ferric wheel is[15,20]

$$H = -J\left(\sum_{i=1}^{5}\mathbf{S}_i\cdot\mathbf{S}_{i+1} + \mathbf{S}_6\cdot\mathbf{S}_1\right) + \sum_{i=1}^{6}\mathbf{S}_i\cdot\mathbf{D}_i\cdot\mathbf{S}_i + \sum_{i=1}^{6}\mathbf{S}_i\cdot\mathbf{g}_i\cdot\mathbf{B} \quad (1)$$

consisting of the standard terms: the Heisenberg term, a zero-field-splitting (ZFS) term due to the ligand-field interaction, and the Zeeman term, respectively. A dipole−dipole interaction will be considered later. Without ZFS, the energy levels and wave functions can be calculated by using the irreducible tensor

(21) Yvon, K.; Jeitschko, W.; Erwin, P. *J. Appl. Crystallogr.* **1997**, *10*, 73.
(22) Abragam, A.; Bleaney, B. *Electron Paramagnetic Resonance of Transition Ions*; Clarendon Press: Oxford, U.K., 1970.
(23) Steinmeyer, F.; Kleiner, R.; Müller, P.; Müller, H.; Winzer, K. *Europhys. Lett.* **1994**, *25*, 459.
(24) Waldmann, O.; Steinmeyer, F.; Müller, P.; Neumeier, J. J.; Régi, F. X.; Savary, H.; Schneck, J. *Phys. Rev. B* **1996**, *53*, 11825.

operator approach.[25] An exact calculation including the ZFS is beyond the limits of today's computers. We therefore calculated the ZFS within first-order perturbation theory for all energy levels. We used the scheme of Bloch,[25] which is particularly suitable, since about 40% of the zero-order states are degenerate, besides the trivial degeneracy in the magnetic quantum number *M*. Matrix elements of the ZFS were calculated using irreducible tensor operator techniques.[25]

For nondegenerate spin states this approach is equivalent to the well-known method of introducing an effective spin Hamiltonian[25]

$$H_S = \mathbf{S}\cdot\mathbf{D}_S\cdot\mathbf{S} + \mathbf{S}\cdot\mathbf{g}_S\cdot\mathbf{B} \qquad (2)$$

for each spin state, where S is the spin quantum number. $\mathbf{D}_S$ and $\mathbf{g}_S$ are given by $\mathbf{D}_S = \sum_i a_{S,i}\mathbf{D}_i$ and $\mathbf{D}_S = \sum_i b_{S,i}\mathbf{g}_i$. In general, this approach breaks down in the case of degenerate levels.

The symmetry of eq 1 requires that all the coefficients $a_{S,i}$ and $b_{S,i}$ are identical. Since the tensors $\mathbf{D}_i$ are connected by symmetry operations of the point group of the complexes, only the components parallel to the main symmetry axis survive the summation. $\mathbf{D}_S$ is thus strictly axial irrespective of the actual single-ion symmetry, so that the ZFS can be parametrized by one single parameter. Our calculations show that this is also true for the degenerate states. Therefore, without loss of generality the ZFS term in eq 1 can be replaced by $D\sum_i[S_{i,z}^2 - {}^1/_3 S_i(S_i+1)]$. A similar argument can be applied for the **g**-tensor.

In agreement with ref 20, the following ZFS factors D_S in eq 2 were calculated for the lowest $S = 1, 2, 3$ terms: $D_1 = -13.597D$, $D_2 = -3.091D$, and $D_3 = -1.340D$. To interpret the magnetic anisotropy of $[Na\subset Fe_6(OMe)_{12}(dbm)_6]$, Caneschi et al.[15] developed a procedure with two approximations. First, they replaced eq 1 by an effective Hamiltonian written as a function of the operators $\mathbf{S}_a = \mathbf{S}_1 + \mathbf{S}_3 + \mathbf{S}_5$ and $\mathbf{S}_b = \mathbf{S}_2 + \mathbf{S}_4 + \mathbf{S}_6$, which allowed for a straightforward inclusion of ZFS. The following ZFS factors for the lowest state of each S manifold, corresponding to the configuration $\mathbf{S}_a = \mathbf{S}_b = {}^{15}/_2$, were obtained: $D_1 = -14.4D$, $D_2 = -3.265D$, and $D_3 = -1.409D$. A comparison with the values given above demonstrates that for the $D/|J|$ ratios observed for ferric wheels this approach is as accurate as the exact first-order perturbational treatment since differences are of second order. Furthermore, Caneschi et al. calculated the magnetic susceptibility taking into account only the anisotropic contributions for the configurations $\mathbf{S}_a = \mathbf{S}_b = {}^{15}/_2$ and $\mathbf{S}_a = {}^{13}/_2$, $\mathbf{S}_b = {}^{15}/_2$. By comparison with our curves, this approximation turned out to be of excellent quality.

Additionally, we compared the average susceptibility versus temperature calculated for the isotropic case and with inclusion of a ZFS contribution. The differences were found to be below experimental accuracy, so that within the restrictions of first-order perturbation theory a ZFS contribution cannot be determined from powder susceptibility measurements.

To explore the effects of higher perturbational terms on the ZFS factors D_S of the lowest energy states, we diagonalized the exact matrix representation of eq 1 for a subset of wave functions consisting of the N lowest zero-order states. For $N = 500$ the accuracy of the energy values is already better than 0.05%. These calculations showed that for $|D/J|$ lower than about 0.05 the first-order approximation is accurate, e.g., D_1 increases only by 1.5% for $D/|J| = -0.05$ compared to the first-order value.

(25) Bencini, A.; Gatteschi, A. *Electron Paramagnetic Resonance of Exchange Coupled Systems*; Springer-Verlag: Berlin, Heidelberg, Germany, 1990.

Finally, the dipole−dipole interaction needs to be considered. Its inclusion leads to a contribution $\mathbf{D}_S^{dip}$ to the tensor $\mathbf{D}_S$ in eq 2. Within first-order perturbation theory one may write[25]

$$\mathbf{D}_S^{dip} = \sum_{i<j} c_{S,ij}\mathbf{D}_{ij} \qquad (3)$$

where $\mathbf{D}_{ij}$ is the dipole−dipole interaction tensor[25] and $c_{S,ij}$ are numerical values depending on S. A treatment within first-order perturbation theory is justified since, e.g., for the lowest $S = 1$ state a ZFS as high as $|D_1| = 0.68\,|J|$ can be tolerated. The $c_{S,ij}$ were calculated in a way similar to that described above. Again, the symmetry of the clusters implies that the tensors $\mathbf{D}_S^{dip}$ are strictly uniaxial, i.e., they can be characterized by one single parameter D_S^{dip}. In detail, we obtained $D_1^{dip} = 1.60$ K, $D_2^{dip} = 0.39$ K, and $D_3^{dip} = 0.19$ K for **1**, $D_1^{dip} = 1.54$ K, $D_2^{dip} = 0.38$ K, and $D_3^{dip} = 0.19$ K for **2**. Using the $c_{S,ij}$ calculated with the approximation scheme of Caneschi et al.[15] we found, e.g., for **1**: $D_1^{dip} = 1.72$ K, $D_2^{dip} = 0.42$ K, and $D_3^{dip} = 0.21$ K. As the ligand-field contribution the effects of the dipole−dipole interaction are covered reasonably by their procedure. Henceforward the symbols D and D_S should be understood as to include both the ligand-field and the dipolar contributions.

3.2. Torque Magnetometry. Since torque magnetometry has not been widely applied for the study of magnetic anisotropy of cluster complexes, we will discuss it in more detail in order to provide some feeling for the interpretation of torque measurements and in particular to demonstrate its specific advantages. In a magnetic field, an anisotropic cluster experiences the torque

$$\boldsymbol{\tau} = \mathbf{m}\times\mathbf{B} \qquad (4)$$

where **m** denotes the magnetization vector and **B** the magnetic field vector. For a uniaxial cluster with the symmetry axis parallel to z it is sufficient to consider magnetic fields lying in the xz-plane, so that the torque points in the y direction with a magnitude of

$$\tau = m_z B_x - m_x B_z = (m_z \sin\Theta - m_x \cos\Theta)B \qquad (5)$$

B is the magnitude of the magnetic field, and Θ is the angle between the magnetic field and the z-axis. m_z (m_x) denotes the z (x) component of the magnetization with the magnetic field applied in the xz-plane. A torque susceptibility $\Delta\chi = \chi_z - \chi_x$ is defined by

$$\tau = \Delta\chi B^2 \sin\Theta\cos\Theta \qquad (6)$$

According to eq 1, there are two contributions to the magnetic anisotropy: ZFS and g-factor anisotropy. For **1** and **2** these can be parametrized by the three parameters D, $g_\parallel$, and $g_\perp$. In the absence of ZFS, the principal components of the magnetic susceptibility tensor are given by $\chi_\sigma(T) = g_\sigma^2 f(T)$, defining a function $f(T)$ which is independent of $\sigma = \parallel, \perp$. Then, $\Delta\chi(T) = \Delta g^2 f(T)$ with $\Delta g^2 = (g_\parallel^2 - g_\perp^2)$. On the other hand, in the absence of g-factor anisotropy the magnetic susceptibility is given by $\chi_\sigma(T) = g^2 f_\sigma(T)$, yielding $\Delta\chi(T) = g^2 h(T)$ where $h(T) = f_\parallel(T) - f_\perp(T)$. If both ZFS and g-factor anisotropy are present, the torque susceptibility becomes $\Delta\chi(T) = g_\parallel^2 f_\parallel(T) - g_\perp^2 f_\perp(T)$. As has been discussed above, the temperature dependence of the average magnetic susceptibility is not affected by a ZFS, hence the torque susceptibility may be expressed as

$$\Delta\chi(T) = \gamma g^2 h(T) + \Delta g^2 f(T) \qquad (7)$$

where $g^2 = {}^1/_3(g_\parallel^2 + 2g_\perp^2)$ and $\gamma \approx (1 + {}^1/_3\Delta g^2/g^2)$. Equation

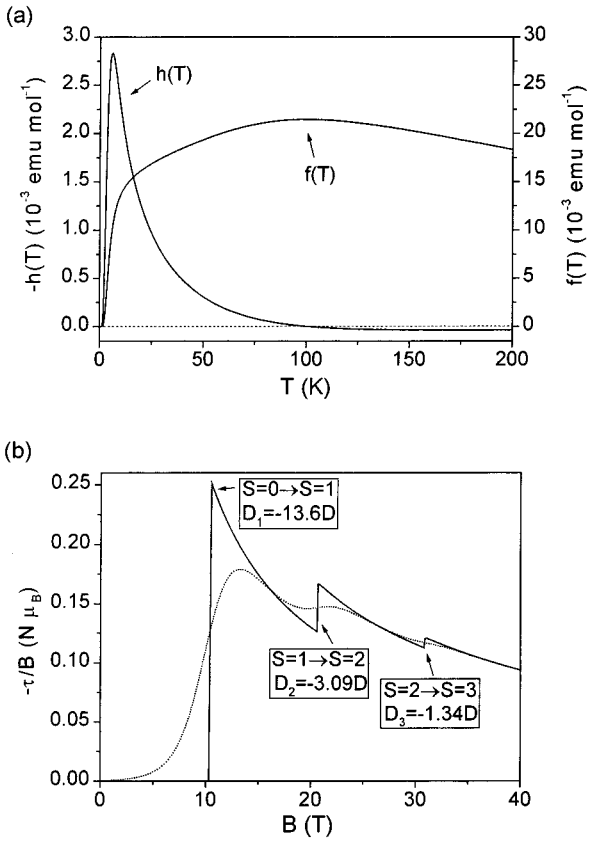

Figure 1. (a) Temperature dependence of the two functions $f(T)$ and $h(T)$ discussed in the text. $f(T)$ was calculated for $J = -20$ K and $h(T)$ for $J = -20$ K and $D = -0.25$ K. (b) Magnetic field dependence of the torque at zero temperature (solid line) and $T = 1.7$ K (dotted line). Parameters were $J = -20$ K and $D = -0.25$ K.

6 shows that the torque susceptibility is composed of the two magnetic anisotropy contributions in a simple manner. It is therefore an excellent source of information for their determination.

The temperature dependencies of the two functions $f(T)$ and $h(T)$ are shown in Figure 1a for a given set of J and D parameters. The behavior of $f(T)$ is known as it is proportional to the average magnetic susceptibility. $h(T)$ exhibits a pronounced maximum at $T \propto |J|$ and is almost zero at higher temperatures. But most importantly, the magnitude of $h(T)$ is a direct measure of D. The different temperature dependencies of $h(T)$ and $f(T)$ suggest the following straightforward procedure for the determination of J, D, and Δg^2: J can be determined from the temperature scale of the torque susceptibility, Δg^2 from the magnitude at temperatures $T \gg |J|$, and then D from the magnitude at $T \approx |J|$.

The magnetic field dependence of the torque $\tau(B)$ cannot be decomposed into a ZFS and g-factor contribution as the torque susceptibility. For negligible g-factor anisotropy (which is the case of interest in this work) and temperatures well below $|J|$, $\tau(B)/B$ behaves as shown in Figure 1b. In the calculations we took into account only the lowest $S = 0$, 1, 2, and 3 states. At zero temperature, a "torque step" occurs for each level crossing. For temperatures $T > 0$ the torque steps are thermally smeared out. Similar to the familiar magnetization steps the location of the torque steps is fixed by the coupling constant and the ZFS parameters D_S of the individual spin states. Due to the ZFS the field values of the steps depend on the angle Θ, but for $\Theta = 54.7°$ we found it to be determined practically by $|J|$ only. In contrast to magnetization steps, however, the magnitude of each torque step is directly related to the ZFS factor of the relevant spin state: For magnetic fields between the level crossing fields B_S and B_{S+1} the ground state belongs to the spin state S whose anisotropy is controlled by D_S. In our case with a $S = 0$ cluster ground state the height of the first torque step is determined by the ZFS factor D_1 of the lowest $S = 1$ state, the height of the second torque step is related to D_2, and so on. $\tau(B)$ thus allows a direct determination not only of the coupling constant but also of the individual ZFS of each spin level. This is probably the most advantageous property of torque magnetometry.

This discussion of the torque is valid as long as the conditions for the validity of first-order perturbation theory are fulfilled. But it is obvious that the utility of torque magnetometry is not limited to this case.

3.3. Neutron Cross Section. The relevant differential neutron scattering cross section for a transition between two levels $|\alpha SM\rangle$ and $|\alpha' S' M'\rangle$ of a spin cluster is given by:[26]

$$\frac{\partial^2\sigma}{\mathrm{d}\Omega\,\mathrm{d}E} = C(Q,T)\sum_{\mu,\nu}\left\{\delta_{\mu\nu} - \frac{Q_\mu Q_\nu}{Q^2}\right\}\sum_{i,j}\{gF(Q)\}^2 \times \exp(i\mathbf{Q}(\mathbf{R}_i - \mathbf{R}_j))\langle\alpha SM|S_i^\mu|\alpha' S' M'\rangle\langle\alpha' S' M'|S_i^\nu|\alpha SM\rangle \quad (8)$$

where

$$C(Q,T) = \frac{1}{4}\frac{N}{Z}\left\{\frac{\gamma e^2}{m_e c^2}\right\}\frac{k'}{k}\exp(-2W(Q,T)) \times \exp\left\{\frac{-E_{\alpha SM}}{k_B T}\right\}\delta(\hbar\omega + E_{\alpha SM} - E_{\alpha' S' M'})$$

Here, α denotes additional necessary quantum numbers, i and j refer to the six Fe(III) ions of the cluster, k and k' are the wavenumbers of the incoming and scattered neutrons, $\mathbf{Q}$ is the scattering vector, $\exp(-2W(Q,T))$ is the Debye−Waller factor, g is the Landé factor, $F(Q)$ is the magnetic form factor of Fe(III), $\mathbf{R}_i$ is the position vector of the ith Fe(III) ion, μ and ν stand for the spatial coordinates x, y, and z, and $\gamma = -1.91$ is the gyromagnetic ratio of the neutron. The remaining symbols have their usual meaning.

The matrix elements of S_i^μ and S_i^ν are best evaluated by using irreducible tensor operator techniques.[25] Since our experiments are performed on a powdered sample with random orientation of the hexamer with respect to $\mathbf{Q}$, the cross section has to be averaged in Q space. The evaluation of the matrix elements $\langle\alpha SM|S_{i,j}^{\mu,\nu}|\alpha' S' M'\rangle$ in eq 8 is rather involved. The spin Hamiltonian in eq 1 is not diagonal in the intermediate spin quantum numbers $\alpha = S_{12}S_{123}S_{1234}S_{12345}$.[27] The cluster wave functions are thus linear combinations of the possible intermediate spins for a given S state. For a $S = 0$ and 1 cluster state there are 111 and 315 terms in the wave function, respectively. We therefore used the approximate wave function of Caneschi et al.[15] with the configurations $\mathbf{S}_a = \mathbf{S}_b = {}^{15}/_2$ and $\mathbf{S}_a = {}^{13}/_2$, $\mathbf{S}_b = {}^{15}/_2$ for the evaluation of the matrix elements in eq 8, and in particular for the calculation of the Q dependence of the scattering intensity. As was demonstrated above, these wave functions represent a reasonable approximation at least as far as energy splittings are concerned. For the evaluation of the

(26) Marshall, W.; Lovesey, S. W. *Theory of Thermal Neutron Scattering*; Clarendon Press: Oxford, 1971.
(27) Gatteschi, D.; Pardi, L. *Gazz. Chim. Ital.* **1993**, *123*, 231.
(28) Clemente-Juan, J. M.; Palii, A. V.; Tsukerblat, B. S., Georges, R. In *Molecular Magnetism: From Molecular Assemblies to Devices*; Coronado, E., Delhaès, P., Gatteschi, D., Miller, J. S., Eds.; Kluwer Academic Publishers: Dordrecht, Netherlands, 1996; pp 85−110.

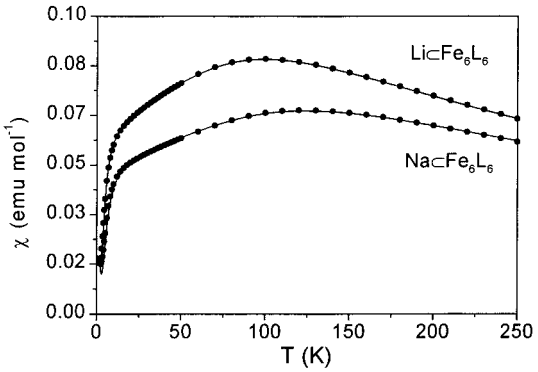

Figure 2. Temperature dependence of the powder magnetic susceptibility of **1** and **2**. Solid lines represent fits with the parameters $J = -20$ K, $\rho_{imp} = 0.1\%$ for **1** and $J = -24.9$ K, $\rho_{imp} = 0.1\%$ for **2**.

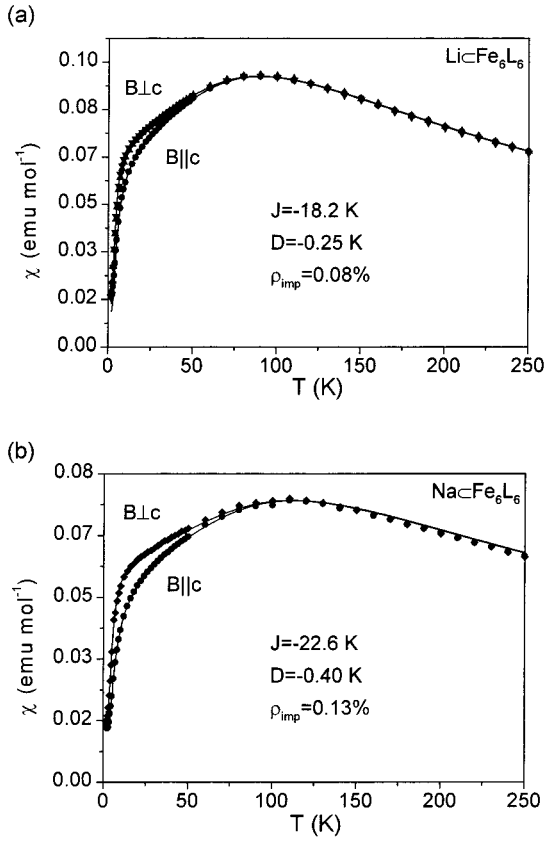

Figure 3. Temperature dependence of the magnetic susceptibility of single crystals of (a) **1** and (b) **2** for magnetic fields applied parallel and perpendicular to the molecular S_6 symmetry axis, respectively. Solid lines represent fits using a first-order calculation (see text). Parameters are given in the panels.

differential neutron cross section in eq 8 within the reduced basis we made use of the program ANIMAG[28] which is of general usability.

4. Experimental Results

The magnetic susceptibility of powder samples of **1** and **2** is shown in Figure 2 as a function of temperature. The temperature dependencies exhibit the behavior expected for a hexanuclear ring of antiferromagnetically coupled Fe(III) ions with an $S = 0$ ground state.[15,20] Broad maxima are detected at 100 K (**1**) and 120 K (**2**) accompanied by a sharp drop of the susceptibilities at low temperatures. Figure 3 presents the susceptibility of single crystals of **1** and **2** with the magnetic field applied perpendicular and parallel to the molecular S_6 axis. A pronounced magnetic anisotropy with $\chi_{||} < \chi_{\perp}$ for both **1** and **2** is observed. Within experimental accuracy, a *g*-factor anisotropy could not be detected.

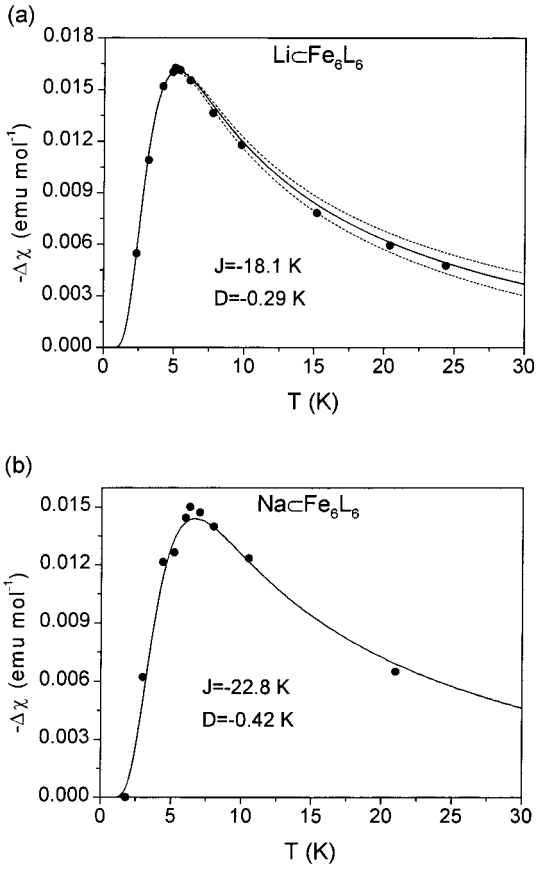

Figure 4. Temperature dependence of the torque susceptibility of single crystals of (a) **1** and (b) **2**. Solid lines represent fits using a first-order calculation (see text) with parameters given in the panels. For the dashed curves, an additional *g*-factor anisotropy was taken into account with $\Delta g/g = 0.01$ (lower dashed curve) and $\Delta g/g = -0.01$ (upper dashed curve).

Figure 4 shows the temperature dependence of the torque susceptibility for **1** and **2**. The torque susceptibilities are negative in accord with $\chi_{||} < \chi_{\perp}$. They exhibit pronounced maxima at 5 K (**1**) and 6.5 K (**2**), respectively. The magnetic field dependence of the torque at 1.7 K is shown in Figure 5. The torque is essentially zero at low fields as expected for a nonmagnetic $S = 0$ ground state. At higher fields, the torque increases, passes inflection points at approximately 9 T (**1**) and 11.5 T (**2**), and reaches a maximum at approximately 12 T (**1**) and 15 T (**2**). The overall field dependence somewhat resembles a magnetization step indicating a level crossing. However, the torque decreases again at higher fields as is seen in Figure 5a, which is typical for a torque step.

In Figure 6 we report the INS spectra of the polycrystalline sample **6** at temperatures $T = 1.8$, 10, and 30 K and $Q = 1.0$ Å^{-1}. They cover the energy-transfer range $\hbar\omega$ from 0 to 35 K on the neutron-energy loss side. The experimental resolution is 1 K at the elastic peak position and increases linearly with increasing energy transfer $\hbar\omega$. The 1.8 K spectrum is best reproduced with a linear background and three Gaussians, I−III, of increasing width centered at 11.8, 18.0, and 28.3 K, respectively (see bottom spectrum of Figure 6). At 10 and 30 K a hot transition α at 32.1 K can be identified. All three spectra have a relatively high background scattering intensity as indicated by the dotted lines in the figure.

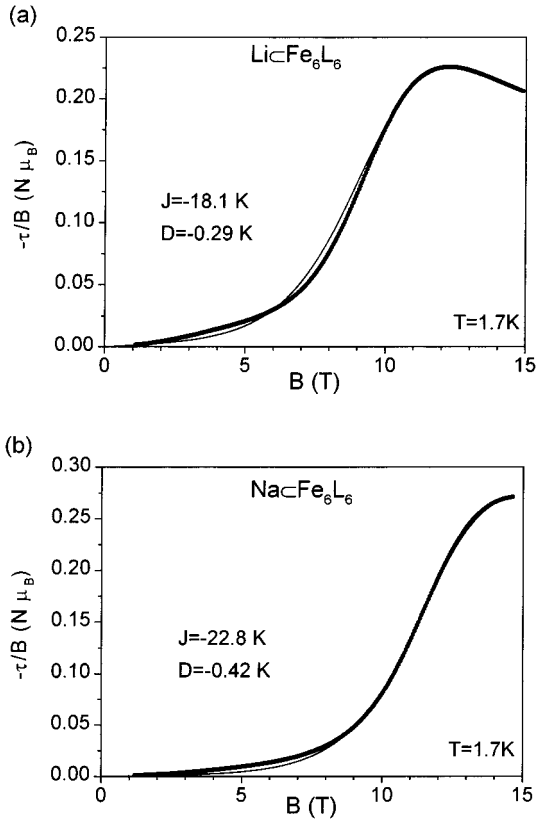

Figure 5. Magnetic field dependence of the torque of single crystals of (a) **1** and (b) **2** at 1.7 K. The data points form the thick "lines". Solid lines represent fits calculated from the lowest $S = 0$, 1, 2 states with parameters given in the panels.

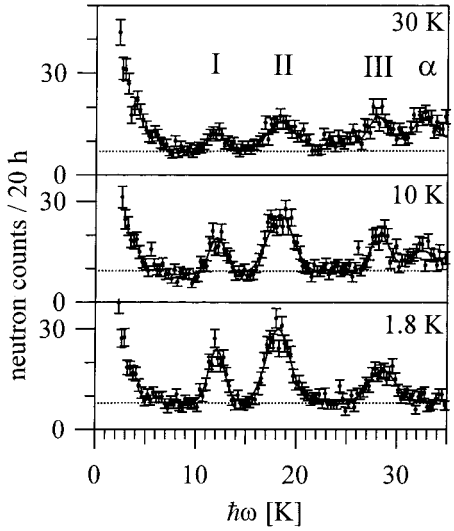

Figure 6. Neutron-energy loss INS spectra of sample **6** measured on the DrüchaL spectrometer with fixed analyzer energy of 2.7 meV. The experimental points are shown for three temperatures $T = 1.8$, 10, and 30 K at $Q = 1.0$ Å^{-1}. The least-squares Gaussians fits are shown as solid lines. The peaks are labeled at the top of the figure.

The temperature dependencies of the scattering intensities of transitions I, II, III, and α are presented in Figure 7a. The data points were obtained from the least-squares Gaussian fits shown in Figure 6. The scattering intensities for transitions I, II, and III at $T = 1.8$ K are normalized to 1.0, whereas for transition α the normalization is done at $T = 10$ K to match the Boltzmann factor of the first excited spin manifold at that temperature. The dependence of the INS intensity on the scattering vector Q is depicted in Figure 7b. The intensity of transition I is normalized to 1.0 at $Q = 1.0$ Å^{-1}.

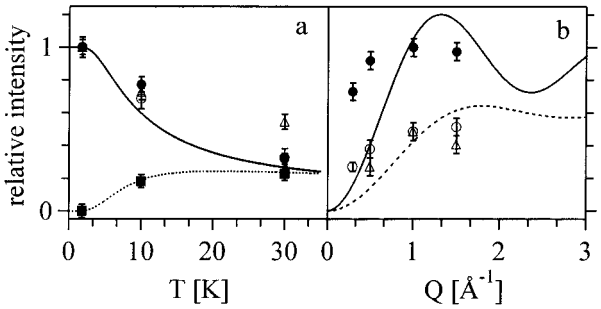

Figure 7. (a) Scattering intensities of transitions I (solid circles), II (open circles), III (open triangles), and α (solid squares) as a function of T. The data were normalized to 1.0 at $T = 1.8$ K for transitions I, II, and III; to the calculated Boltzmann factor for the first excited spin manifold at $T = 10$ K for transition α. The solid and dotted lines are the Boltzmann factors for the ground and first excited spin manifold as a function of T. (b) Scattering intensities of transitions I (solid circles), II (open circles), and III (open triangles) as a function of the scattering vector Q. The solid and dashed lines represent the calculated intensity behavior of transition I and II as a function of Q. The intensity of transition I is normalized to 1.0 at $Q = 1.0$ Å^{-1}.

5. Analysis and Discussion

5.1. Energy Splittings and Parameters for Complexes 1 and 2 Derived from Magnetic Measurements. The temperature dependence of the powder magnetic susceptibility of **1** and **2** can be fitted accurately by the isotropic parts of eq 1, additionally taking into account a small contribution of paramagnetic $S = {}^5/_2$ impurity parametrized by a mole fraction ρ (see Figure 2). The antiferromagnetic coupling constants thus obtained are

$$\begin{aligned} &\textbf{1} \text{ (powder):} \quad J = -20.0(4) \text{ K} \\ &\textbf{2} \text{ (powder):} \quad J = -24.9(5) \text{ K} \end{aligned} \tag{9}$$

These values compare well with those reported for other ferric wheels.[7,15,17,20] They are 2 K larger than those obtained for the same complexes in different crystal environments of **3** ($J = -18.1$ K) and **4** ($J = -23$ K).[20] The magnetic anisotropy, as revealed by the crystal susceptibility measurements, can be accurately reproduced by our first-order calculations, yielding the following parameter values (see Figure 3):

$$\begin{aligned} &\textbf{1} \text{ (crystal):} \quad J = -18.2(4) \text{ K}, D = -0.25(4) \text{ K} \\ &\textbf{2} \text{ (crystal):} \quad J = -22.6(7) \text{ K}, D = -0.40(6) \text{ K} \end{aligned} \tag{10}$$

The coupling constants for the crystal samples are smaller than the values observed for the powder samples. They are in better agreement with those derived from the polycrystalline samples **3** and **4**.

The temperature dependence of the torque susceptibility is well reproduced by a first-order calculation taking into account only the ZFS contribution to the magnetic anisotropy (Figure 4). The following parameters for the crystal samples were determined:

$$\begin{aligned} &\textbf{1} \text{ (crystal):} \quad J = -18.1(4) \text{ K}, D = -0.29(3) \text{ K} \\ &\textbf{2} \text{ (crystal):} \quad J = -22.8(3) \text{ K}, D = -0.42(4) \text{ K} \end{aligned} \tag{11}$$

The agreement with the parameters derived from the crystal magnetic susceptibility is excellent. In Figure 4a we also draw the curves calculated with an additional g-factor anisotropy of

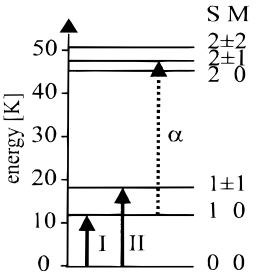

Figure 8. Experimentally determined energy-splitting pattern of the lowest cluster states of $Na[Fe_6\{N(CH_2CH_2O)_3\}_6]Cl$ in sample **6** derived from the INS experiment with corresponding wave functions in the first-order approximation. Observed cold and hot transitions are given as full and broken arrows, respectively. The labels of the transitions are those used in Figure 6.

$\Delta g/g = \pm 0.01$. Evidently, the *g*-factor anisotropy is very small, justifying its neglect in our analysis. Taking into account only the lowest $S = 0$, 1, 2 states the magnetic field dependence of the torque is nicely reproduced (Figure 5) and yields the same parameters, eq 11. The esd given in eq 11 are those obtained from $\tau(B)$.

5.2. Energy Splittings and Parameters for Complex 6 Derived from INS. As discussed in section 2.1 the sample **6** used for the INS study was prepared from CH_2Cl_2 instead of $CHCl_3$ and contains a sizable impurity phase. The inelastic transition III in the spectra of Figure 6 is attributed to this impurity on the basis of its energy. First we note that it must be due to a polynuclear Fe(III) species, because there are no ground-state splittings of this magnitude in a mononuclear complex. A Fe_6 wheel can be ruled out because the energy is too high for $S = 0 \rightarrow S = 1$ excitations. In addition, the magnetic susceptibility of sample **6** clearly indicates an impurity with an odd number of electrons. From the synthesis an Fe_5 wheel appears plausible. The calculated exchange splitting of an Fe_5 wheel with spin Hamiltonian parameters similar to those found in the Fe_6 wheel yields an $S = {}^1/_2$ cluster ground state separated by 29.2 K from the next higher $S = {}^3/_2$ state. This splitting is close enough to 28.3 K, the energy of band III in Figure 6, to make the tentative assignment.

Turning now to the features in the INS spectrum which are due to $[Na\subset Fe_6\{N(CH_2CH_2O)_3\}_6]Cl$, we derive the energy level diagram in Figure 8 from the observed positions of the bands I, II, α (Figure 6) and their *T* dependence (Figure 7a). The observed *T* and *Q* dependence shown in Figure 7 identifies these inelastic features as magnetic excitations. Vibrational bands do not decrease with *T*, and their intensity roughly increases with Q^2.[26] We are thus safe in assigning the bands I, II, and α to $[Na\subset Fe_6\{N(CH_2CH_2O)_3\}_6]Cl$. The agreement of their observed *T* dependence with the calculated Boltzmann factors is excellent (Figure 7a).

There is an additional complication in this triclinic salt. The Fe_6 wheel is not a regular hexagon by symmetry. In the crystal structure $[Na\subset Fe_6\{N(CH_2CH_2O)_3\}_6]Cl\cdot 2CH_2Cl_2$ the Fe−Fe distances show small variations between 3.21 and 3.23 Å. We should expect similar variations in the crystal structure of the dried sample. We have made numerous test calculations of the energy splitting in distorted hexagons. They show that the splitting of the lowest energy cluster levels is not affected by these distortions. It only depends on the mean values of the spin Hamiltonian parameters.

The assignment of the two energy levels at 11.8 K (band I) and 18.0 K (band II) to the cluster levels $|10\rangle$ and $|1 \pm 1\rangle$, respectively, is based on an intensity argument. Using the cross-section formula eq 8 the $|1 \pm 1\rangle$ excitation is estimated to be roughly twice as intense as the $|10\rangle$ excitation, in agreement with the observed behavior (see Figure 7b). From the energies of I and II we directly obtain the parameters as follows: In first order the baricenter corresponds to $0.6917|J|$ and the splitting to $-13.597D$. We get

$$\mathbf{6}: \; J = -23.0(3)\ \text{K}, \; D = -0.45(1)\ \text{K} \qquad (12)$$

similar to the parameters for the same complex **2** in the crystalline hexagonal form.

With the parameters in eq 12 the transitions $|1 \pm 1\rangle \rightarrow |2 \pm 2\rangle$, $|10\rangle \rightarrow 20\rangle$, and $|10\rangle \rightarrow |2 \pm 1\rangle$ are calculated at 32.6, 33.1, and 34.5 K, respectively. They are unresolved in the band α centered at 32.1 K. The observed intensity ratio of bands α and II at 30 K and $Q = 1.0$ Å^{-1} is 0.6(2), in excellent agreement with the calculated ratio of 0.5 using the cross-section formula eq 8. Additional hot intensity is calculated at 27.0 and 28.4 K for the transitions $|1 \pm 1\rangle \rightarrow |20\rangle$ and $|1 \pm 1\rangle \rightarrow |2 \pm 1\rangle$, $|10\rangle$, respectively. They coincide with band III, thus explaining the considerable intensity at 30 K in Figure 7b. Finally, the hot transition $|10\rangle \rightarrow |1 \pm 1\rangle$, expected at 6.2 K is not observed in the spectra of Figure 6 due to its low calculated intensity using eq 8.

We note in Figure 7b that the agreement between the observed and calculated *Q* dependence of intensity for transition I and II is poor. We ascribe this to the approximate nature of our cluster wave functions resulting from the restriction to $\mathbf{S}_a = \mathbf{S}_b = {}^{15}/_2$ and $\mathbf{S}_a = {}^{13}/_2$, $\mathbf{S}_b = {}^{15}/_2$ configurations. While the energy splittings are well approximated by this restricted model, the INS intensities are much more sensitive to the deficiencies in the wave functions.[29]

A final comment concerns the fact that a nondeuterated sample was used for this INS study. We ascribe the relatively high background in the spectra of Figure 6 to incoherent scattering from the hydrogen atoms. But this does not prevent us from observing magnetic cluster excitations in the energy range up to 35 K. Similar observations have been made for $[Fe_8O_2(OH)_{12}(tacn)_6]^{8+}$ and $Mn_{12}O_{12}(O_2CCH_3)_{16}(H_2O)_4$.[30,31] There is obviously an energy range in which the density of vibrational states with a significant hydrogen contribution is sufficiently small, so that magnetic excitations are not swamped. We are presently exploring the width of this window. It opens up the possibility to explore numerous spin clusters by INS for which deuteration is prohibitive.

5.3. Discussion of Results. Since we have investigated the two complexes $[Li\subset Fe_6L_6]^+$ and $[Na\subset Fe_6L_6]^+$ in different environments, a comparison of the determined parameters and a discussion in relation to their structure is in order.

The most conspicuous observation is the significant difference of the coupling constants of the hexagonal salts **1** and **2** in the powder (see eq 9) and in the crystalline form (see eq 10, 11). We ascribe this to structural changes of the clusters resulting from the loss of $CHCl_3$ molecules upon drying. The volume of the hexagonal unit cell shrinks about 50% in this process, and the density increases by typically 30%. It is thus reasonable to assume a distortion of the cluster upon loss of $CHCl_3$. In contrast to the hexagonal salts, the unit cell parameters of the triclinic salt are almost preserved upon drying. As a consequence we

(29) Andres, H.; Clemente-Juan, J.; Aebersold, M.; Güdel, H.-U.; Coronado, E.; Büttner, H.; Kearly, G.; Melero, J.; Burriel, R. *J. Am. Chem. Soc.*, in press.
(30) Caciuffo, R.; Amoretti, G.; Murani, A.; Sessoli, R.; Caneschi, A.; Gatteschi, D. *Phys. Rev. Lett.* **1998**, *81*, 4744.
(31) Mirebeaum, I.; Hennion, M.; Cassalta, H.; Andres, H.; Güdel, H. U.; Irodiva, A. V.; Caneschi, A. *Phys. Rev. Lett.*, submitted.

do not expect a large geometry and size change of the cluster. This is reflected in the coupling constant of **6**, which compares quite nicely with that of **2** in the crystalline form. The coupling constant J is thus a good measure of the cluster size and geometry.

The good agreement of the ZFS parameters determined from torque and INS is surprising at first, since it is generally believed that bulk techniques sample the whole spectrum while spectroscopic techniques detect the lowest states. However, in contrast to magnetic susceptibility the torque susceptibility is sensitive only to the lowest few states, as indicated by the pronounced maximum of $h(T)$ at $T \approx |J|$ (see Figure 1a). The four lowest spin states are sufficient to reproduce $h(T)$ with high accuracy in the full temperature range. Even the lowest $S = 1$ state alone accounts for the maximum of $h(T)$. Furthermore, as explained at length in section 3.2, the field dependence of the torque allows a sampling of the individual ZFS parameters of each spin state. In our experiments we reached the first torque step, thus detecting D_1. Therefore, the torque parameters mainly reflect the magnitude of D_1, as so does INS.

In ref 20 the perchlorate salts of the same two complexes $[Li\subset Fe_6L_6]^+$ (**3**) and $[Na\subset Fe_6L_6]^+$ (**4**) were studied, together with the alkali free complex $[Fe_6L_6]$ (**5**). Since the coupling reflects the cluster geometry, and since the coupling constants of the crystals of **1** and **2** are very close to those of the polycrystalline samples of **3** and **4**, we conclude that **3** and **4** contain ferric wheels of very similar geometry to our samples. We can thus compare the magnetic parameters of the series $[Li\subset Fe_6L_6]^+$, $[Na\subset Fe_6L_6]^+$, and $[Fe_6L_6]$ determined in our work and in ref 20 and establish a correlation with the structural parameters.

The coupling constants $J = -18, -23, -31.5$ K, respectively, increase in this series along with the Fe−O−Fe angles of 103.4°, 104.9°, and 105.3°, as already mentioned in ref 20. For $[Li\subset Fe_6L_6]^+$ and $[Na\subset Fe_6L_6]^+$ the average of the angles of each bridge of the di-μ-oxo unit is given (101.0°/105.9° for $[Li\subset Fe_6L_6]^+$ and 103.3°/106.4° for $[Na\subset Fe_6L_6]^+$). The value for $[Fe_6L_6]$ is taken from ref 20. On the other hand, no significant correlation to the Fe−O distance is found. This observation fits into the recent conclusion that in related di-μ-oxo-bridged Fe(III) complexes the Fe−O−Fe angle plays the most important role in determining the coupling constant.[32]

Along with the coupling constant we note that also the ZFS, expressed for example as D_1, increases with increasing Fe−O−Fe angle in the series $[Li\subset Fe_6L_6]^+$, $[Na\subset Fe_6L_6]^+$, $[Fe_6L_6]$: $D_1 = 3.9$, 5.8, 11.8 K, respectively. This indicates a novel correlation between ligand-field interactions and exchange interactions in these ferric wheels. As this study is based solely on three complexes, it is clear that it is difficult to perform a more detailed discussion. More work is necessary. However, since D_1 is related to the ZFS of the individual Fe(III) ions, it reflects the crystal-field anisotropy at the Fe(III) centers. By varying the Fe−O−Fe angle the σ and π interactions of the oxygen 2s and 2p electrons with the d electrons of Fe(III) are affected. Both the kinetic exchange and the single-ion anisotropy depend on these interactions; hence the observed correlation between the values of J and D is not unexpected.

After submission of this paper a rather related work by Cornia et al. appeared.[33] These authors performed torque measurements on the cyclic clusters $[LiFe_6(OMe)_{12}(dbm)_6]^+$ and $[NaFe_6(OMe)_{12}(dbm)_6]^+$. In these compounds the magnetic parameters for the coupling and the ZFS are also controlled by the alkaline ion. Additionally they presented an approximate interpretation of the field dependence of the torque at low temperatures.

Acknowledgment. Financial support by the Bayerisches Langzeitprogramm "Neue Werkstoffe", the Deutsche Forschungsgesellschaft, and the Swiss National Science Foundation is gratefully acknowledged.

IC9906510

(32) Le Gall, F.; Biani, F. F.; Caneschi, A.; Cinelli, P.; Cornia, A.; Fabretti, A. C.; Gatteschi, D. *Inorg. Chim. Acta* **1997**, *262*, 123.
(33) Cornia, A.; Affronte, M.; Jansen, A. G. M.; Abbati, G. L.; Gatteschi, D. *Angew. Chem.* **1999**, *111*, 2409.